Human Molecular Genetics, 2011, Vol. 20, No. 21 ***4187–4195***
doi:10.1093/hmg/ddr346
Advance Access published on August 10, 2011

MeCP2 Rett mutations affect large scale chromatin organization

Noopur Agarwal[1,†,‡], Annette Becker[2,†], K. Laurence Jost[1,2], Sebastian Haase[1,¶], Basant K. Thakur[3], Alessandro Brero[1], Tanja Hardt[1,§], Shinichi Kudo[4], Heinrich Leonhardt[5], and M. Cristina Cardoso[1,2,*]

[1]Max Delbrück Center for Molecular Medicine, Berlin 13125, Germany, [2]Department of Biology, Technische Universität Darmstadt, Darmstadt 64287, Germany, [3]Department of Pediatric, Hematology and Oncology, Medical School Hannover, Hannover 30625, Germany, [4]Hokkaido Institute of Public Health, Sapporo 060-0819, Japan and [5]Department of Biology, Ludwig Maximilians University Munich, Planegg-Martinsried 82152, Germany

Rett syndrome is a neurological, X chromosomal-linked disorder associated with mutations in the *MECP2* gene. MeCP2 protein has been proposed to play a role in transcriptional regulation as well as in chromatin architecture. Since MeCP2 mutant cells exhibit surprisingly mild changes in gene expression, we have now explored the possibility that Rett mutations may affect the ability of MeCP2 to bind and organize chromatin. We found that all but one of the 21 missense MeCP2 mutants analyzed accumulated at heterochromatin and about half of them were significantly affected. Furthermore, two-thirds of all mutants showed a significantly decreased ability to cluster heterochromatin. Three mutants containing different proline substitutions (P101H, P101R and P152R) were severely affected only in heterochromatin clustering and located far away from the DNA interface in the MeCP2 methyl-binding domain structure. MeCP2 mutants affected in heterochromatin accumulation further exhibited the shortest residence time on heterochromatin, followed by intermediate binding kinetics for clustering impaired mutants. We propose that different interactions of MeCP2 with methyl cytosines, DNA and likely other heterochromatin proteins are required for MeCP2 function and their dysfunction lead to Rett syndrome.

INTRODUCTION

Rett syndrome (RTT, MIM 312750) is a post-natal neurological disorder, with an incidence of ~1/10 000 female births. The females develop normally until 6–18 months of age, but after that, the growth is drastically slowed down, followed by the development of stereotypical hand movements, autistic behavior, loss of speech and motoric skills, respiratory disorders etc. Mutations in the chromosome Xq28 region corresponding to the *MECP2* gene have been shown to be linked to the disease (1).

MeCP2 recognizes methylated cytosines (5 mC) via a highly conserved methyl-cytosine-binding domain (MBD) and is concentrated in the densely methylated pericentric heterochromatin (2). It has also been shown to contribute to transcriptional regulation via its transcriptional repression domain (TRD) interaction with histone deacetylases (3,4). In addition to its role in regulating gene expression, we have recently shown that the MBD of MeCP2 has the ability to reorganize and cluster heterochromatin *in vivo* (5,6). MeCP2 has accordingly been described to compact nucleosomal arrays *in vitro* (7).

Several types of *MECP2* gene mutations including deletions and also duplications have been found in Rett patients (8,9). Whereas the most common mutations, the missense mutations, are mostly clustered within the MBD (amino acids 78–162), the majority of nonsense mutations occur after the MBD predominantly within the TRD (amino acids 207–310; Fig. 1A). In view of the random nature of X chromosome inactivation in females and, hence, the chimeric pattern of cells expressing

*To whom correspondence should be addressed at: Department of Biology, Technische Universität Darmstadt, Schnittspahnstr. 10, D-64283 Darmstadt, Germany. Tel: +49 6151 162377; Fax: +49 6151 162375; Email: cardoso@bio.tu-darmstadt.de
†These authors contributed equally to this work.
‡Present address: BRIC-Biotech Research & Innovation Center, 2200 Copenhagen, Denmark.
¶Present address: Department of Physics, Freie Universität Berlin, 14195 Berlin, Germany.
§Present address: Medical Proteomics Center, Ruhr University, 44801 Bochum, Germany.

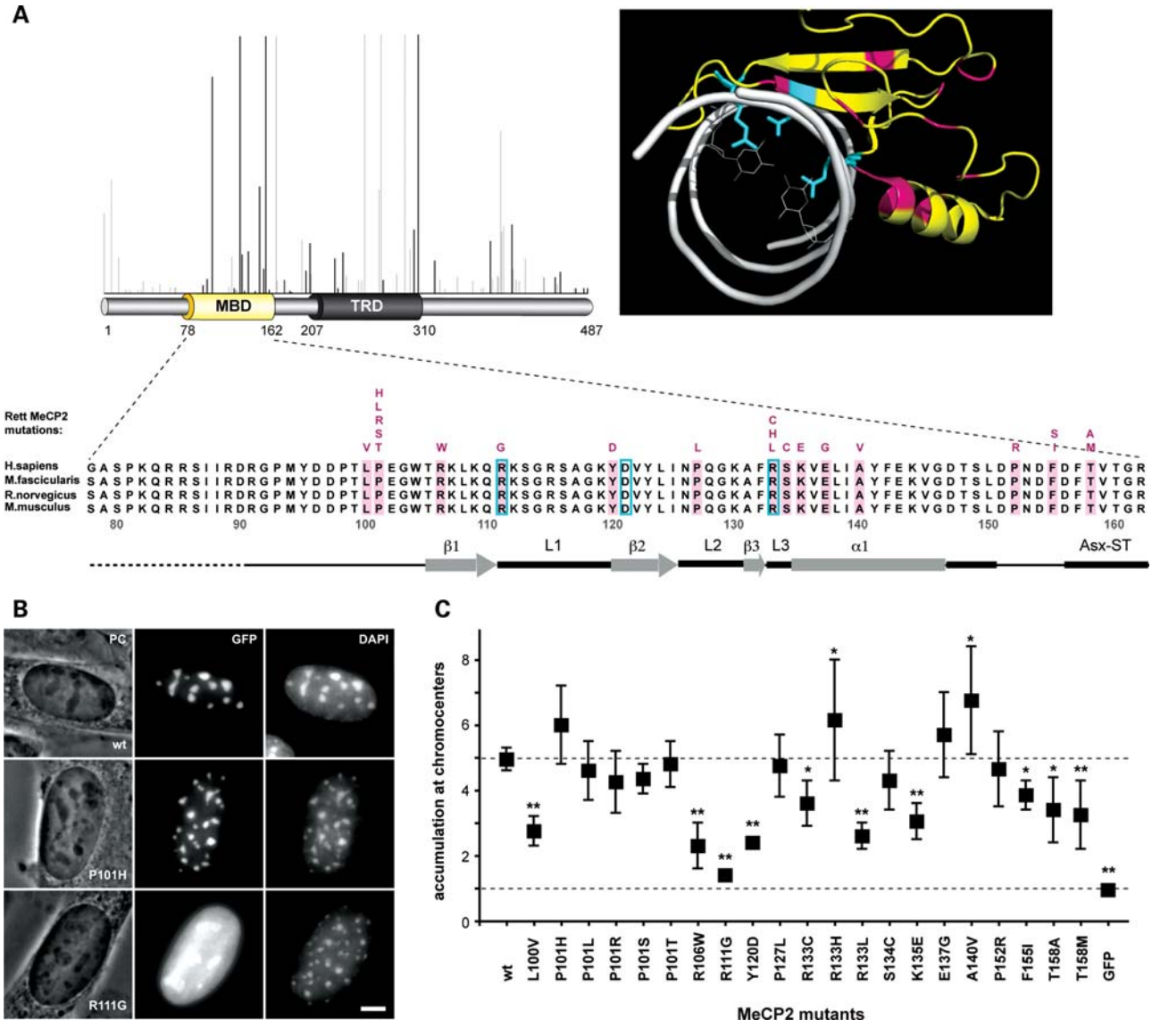

Figure 1. Mutant MeCP2 proteins accumulate at chromocenters *in vivo* to very different extent. (**A**) Top left panel shows the mutation spectrum in Rett patients (IRSA http://mecp2.chw.edu.au/cgi-bin/mecp2/search/printGraph.cgi#MS; last accessed: 15.08.2011), with missense mutations shown in black and others in grey color. Location of individual mutations is indicated in a schematic representation of the MeCP2 protein (numbers are amino acids coordinates). MBD stands for the methyl CpG-binding domain and TRD for the transcription repression domain. Top right panel shows the X-ray structure of the MBD of MeCP2 (displayed in yellow) interacting with its target 5 mC within the DNA double helix (shown in white; PDB accession code 3C2I) (20). Structural data were displayed and annotated using PyMOL software (http://pymol.sourceforge.net/; last accessed: 15.08.2011). The residues that directly interact with the two 5 mC are shown in cyan and the Rett mutations included in our study in pink. Bottom panel: the Rett mutations analyzed are listed (in pink) above the corresponding wild-type amino acid within the sequence of MeCP2 MBD. The location of the defined α-helix (α1), β-strands (β1 and β2) and loops/Asx-ST motif (bold black line) is illustrated below the protein sequence (19,20). (**B**) Representative maximum intensity projections generated from Z-stacks of mouse myoblasts expressing wild-type MeCP2 and mutants thereof. DNA was counterstained with DAPI. PC, phase contrast. Scale bar: 5 μm. (**C**) The plot shows the fold accumulation at chromocenters of 21 Rett mutants, wild-type MeCP2 and GFP in mouse myoblasts. Asterisks represent statistically significant difference in regard to the wild-type: $^{*}P < 0.05$; $^{**}P < 0.001$. All mutants accumulated significantly different ($P \leq 0.05$) with respect to GFP alone (not shown). The experiment was repeated at least two times with 10 cells per mutant evaluated each time.

wild-type or mutant MeCP2, genotype–phenotype correlations are rather complex (10).

Surprisingly, MeCP2 null mice showed unexpectedly mild gene expression changes, strengthening the relevance of other MeCP2 chromatin functions (11). Similar results were obtained from samples of Rett patients (12,13). In this regard, MeCP2 mutations have recently been shown to affect DNA binding, its capacity to induce compaction of nucleosomal arrays (7,14) as well as its chromatin binding kinetics (15,16). However, the mechanism and regulation of MeCP2-induced higher-order heterochromatin organization is still unclear.

In this study, we have systematically characterized 21 missense Rett MeCP2 mutants in terms of their ability to bind and aggregate pericentric heterochromatin and found several which severely affected one or both of these MeCP2 properties.

RESULTS AND DISCUSSION

Based on our finding that the MBD of MeCP2 clusters heterochromatin and most Rett missense mutations affect this domain, we set out to investigate whether they were impaired in binding to and/or clustering heterochromatin.

We selected Pmi28 mouse myoblasts as our cellular assay system. This cell line was used before to characterize the dose-dependent effect of wild-type MeCP2 on the spatial organization of chromocenters and it expresses very low to undetectable level of endogenous wild-type MeCP2 (5). Moreover, it showed a stable and nearly normal karyotype, with minimal variations in chromocenter number caused by variable numerical chromosome aberrations.

We used mammalian expression constructs containing the mutant human MeCP2e2 isoform cDNAs fused at the C-terminus of the enhanced green fluorescent protein (GFP) coding sequence (17). All missense mutations within the MBD are highlighted in pink in Figure 1A, and the mutated forms of the wild-type residues are indicated above the sequence alignment. Intranuclear localization of the fusion proteins and the induction of chromocenter clustering in transfected cells were assessed by epifluorescence microscopy using AT-selective DNA dyes [Hoechst 33258, DAPI (4′-6′-diamidino-2-phenylindol) or TOPRO-3 iodide (4-[3-(3-methyl-2(3H)-benzothiazolylidene)-1-propenyl]-1-[3-(trimethylammonio)propyl]-, diiodide)] to independently visualize pericentric heterochromatin. As MeCP2 strongly accumulates in these heterochromatic regions, we visualize them as a proxy for how (Rett) mutations in the *MECP2* gene can change its ability to associate with chromatin and to reorganize it.

We first tested these MeCP2 Rett mutants for their protein accumulation at the chromocenters by taking a ratio of average mean intensity of protein bound at chromocenters versus nucleoplasm. The results indicate that all the mutant proteins showed enrichment at chromocenters (ratio was >1), but to very different extents (Fig. 1B and C). R111G mutant protein accumulated to the lowest extent. This mutant has been shown before to exhibit complete loss of function of MeCP2 and to no longer repress Sp1-mediated transcriptional activation of methylated and unmethylated promoters (17). We found that it mislocalizes to the nucleoli (phase-dense regions in Fig. 1B) instead of pericentric heterochromatin, which was further confirmed by staining with the nucleolar marker B23 (data not shown). Concomitantly to the lack of heterochromatin association, this mutant depicted an increased nucleoplasmic pool apparent from the high diffuse signal throughout the nucleus (Fig. 1B). F155S exhibited a similar subcellular distribution and a deficit in the heterochromatin accumulation (Supplementary Material, Fig. S1). Except for P101H, R133H, E137G and A140V, all the other analyzed mutant proteins accumulated at chromocenters less than the wild-type, with more than half significantly affected in their accumulation ability when compared with wild-type (Fig. 1C).

Since several mutants associated less efficiently with heterochromatin, we further addressed whether they would be impaired in their ability to cluster heterochromatin *in vivo*. To assess the degree of heterochromatin clustering in a quantitative manner, we scored the number of chromocenters in cells expressing either GFP-tagged wild-type or mutant MeCP2. By this assay, we address the ability of these proteins to reorganize heterochromatin architecture. In Figure 2, the clustering potential of the proteins is displayed as cumulative frequency curves, which represent the percentage of nuclei with up to a certain number of chromocenters. Cells expressing the Rett mutants P101H, P101R and P152R showed a highly significant increase in chromocenter numbers compared with wild-type MeCP2-expressing cells (Fig. 2). R111G and F155S mutants had the most dramatic effect with completely abolished chromocenter clustering (Fig. 2C and Supplementary Material, Fig. S1). Additionally, 10 more mutants exhibited significantly decreased clustering abilities in comparison with wild-type MeCP2 (Fig. 2B). In contrast, the other mutants behaved similarly to the wild-type. Among them is the A140V exchange that has been reported in association with very mild clinical symptoms (18). Altogether, two-thirds of the Rett MeCP2 missense MBD mutants were significantly affected in clustering potential compared with wild-type MeCP2.

We further tested whether the clustering ability of selected mutants was also conserved in human cells. We performed immunostaining in combination with fluorescence *in situ* hybridization using three DNA probes simultaneously to detect the major pericentric heterochromatin regions that are present in chromosomes 1, 9 and 16 (Supplementary Material, Fig. S2A and B) of human cells expressing either wild-type or mutant MeCP2. The outcome of this analysis essentially confirms the results obtained in mouse cells.

Next, we tested whether the clustering of chromocenters generally reflected the amount of protein that accumulated at these regions. Hence, we plotted the median of chromocenter number versus the average accumulation at chromocenters (Fig. 3A). Mutants falling onto an arbitrary line connecting the negative GFP alone control and the positive wild-type MeCP2 control show an inverse correlation between binding to chromocenters and corresponding numbers of chromocenters, i.e. binding less is accompanied by less clustering. The majority of the mutants were both affected in their binding to chromocenters and in clustering chromocenters (Fig. 3A, pink and blue). This could be a consequence of impaired binding affecting their ability to cluster or, alternatively, these mutations could independently affect both properties. Interestingly, some mutants (P101R, P101H and P152R) were mildly to non-affected in heterochromatin binding but severely affected in clustering of chromocenters (Fig. 3A, green). When we applied the same color code to label the corresponding residues in the MBD structure, these residues mapped to the outer part of the MBD (Fig. 3B). Both residues are located adjacent to structured motifs [P101 to β-sheet 1 (β1) and P152 to α-helix 1 (α1)] and within loops (19,20).

As it has been previously shown that some Rett mutations affected chromatin binding kinetics of MeCP2 *in vivo* (15,16), we performed *in situ* detergent extraction as well as fluorescence photobleaching (FRAP) recovery experiments on mutants affected in either chromatin clustering, binding or both. We chose the A140V mutant that was affected neither in binding nor in clustering of chromatin, P101H which was affected only in clustering and R133L affected in both functions (Fig. 4A). The R133L mutation resulted in higher extractability and a much faster FRAP recovery,

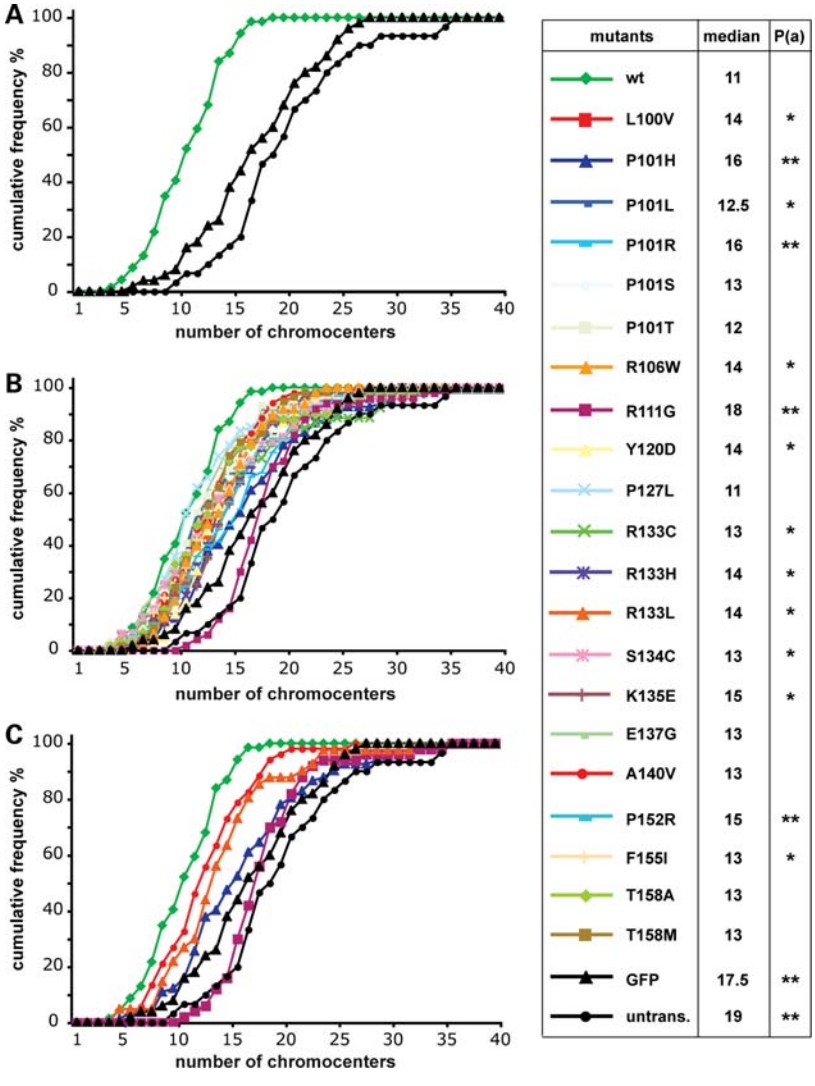

Figure 2. Rett mutant proteins are affected in their ability to cluster chromocenters. Pmi28 mouse myoblasts were transfected with an expression vector coding for GFP or GFP-fused MeCP2 construct as indicated. Z-stacks of images were recorded of nuclei with similar expression levels of the GFP-tagged protein and constant image acquisition parameters. (**A**) The plot shows the percentage of cumulative frequencies of chromocenter numbers in cells expressing GFP-tagged wild-type MeCP2 in comparison to untransfected and GFP-expressing cells. (**B**) Cumulative frequencies of chromocenter numbers in cells expressing each of the 21 GFP-tagged MeCP2 mutants. (**C**) Depicts Rett mutants with extreme phenotypes together with the controls (wild-type MeCP2, GFP and untransfected cells). The table lists the median number of chromocenters for each mutant and depicts the *P*-value with asterisks representing statistically significant difference in regard to the wild-type: $^{*}P < 0.05$; $^{**}P < 0.001$. The experiment was repeated two times with at least 25 cells evaluated per mutant each time.

probably reflecting disruption of binding to 5 mC (Fig. 4B and C). A minimal level of 5 mC seems to be required as a priming event for efficient accumulation of MeCP2 at heterochromatin, as shown by the lack of chromocenter localization of a GFP-tagged MBD fusion in Dnmt1/3a/3b triple knock-out cells (21). Our live-cell kinetic data indeed indicated that although the R133L mutant MeCP2 was still able to accumulate at heterochromatin to a lower extent, it interacted only very transiently and with low affinity. Very similar FRAP kinetics were recently reported for a different mutation of this residue, R133C (15). Both substitutions had comparable heterochromatin clustering potential (Figs 2 and 3), although the R133L exhibited a somehow lower ability to accumulate at heterochromatin (Figs 1 and 3). The *in vivo* accumulation of this mutant at chromatin may be either the result of retaining low-affinity recognition of 5 mC and/or binding to DNA or other heterochromatin-associated proteins. On the other extreme, the A140V mutant protein performed in both assays (*in situ* extraction and FRAP kinetics) as the wild-type (Fig. 4B and C). Importantly, the P101H mutant, which accumulated as the wild-type at heterochromatin but was drastically impaired in clustering chromocenters, had intermediate FRAP kinetics and was also easier to extract from heterochromatin. The FRAP kinetics follow the same trend for the different mutants independently of whether the region photobleached included only chromocenters (Fig. 4C; which measures mostly the contribution of heterochromatin-bound MeCP2) or half of the nucleus (Fig. 4C; with a

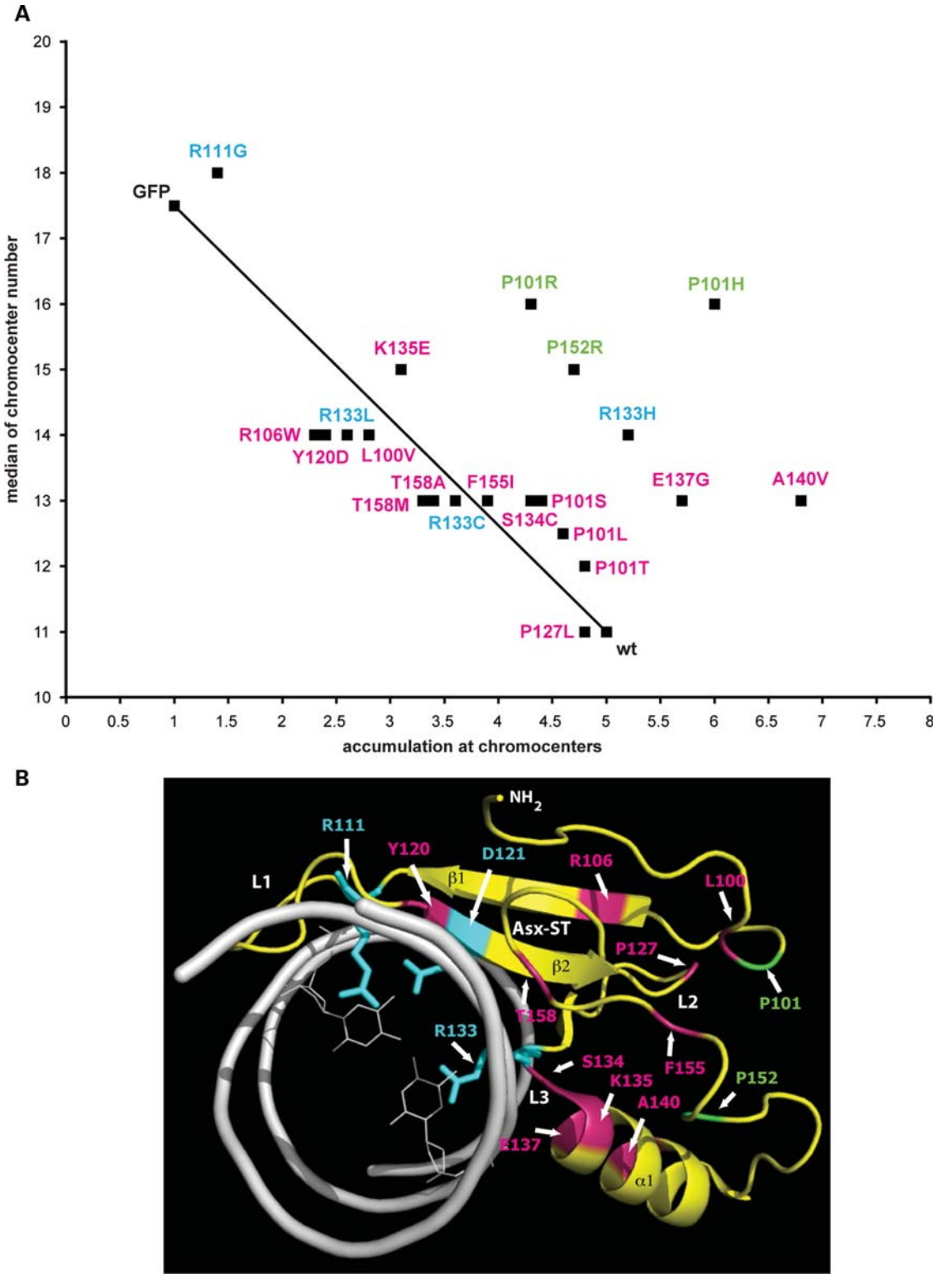

Figure 3. Correlation analysis of chromocenter clustering and accumulation at chromatin. (**A**) Accumulation at chromocenters (Fig. 1) and median of chromocenter number (Fig. 2) were plotted on the *x*- and *y*-axes, respectively. The line connecting the GFP alone and GFP-MeCP2 delineates the inverse relationship between accumulation at chromocenters and chromocenter number (clustering). Mutations of residues directly interacting with 5 mC are shown in blue, and those not directly interacting are illustrated in pink. The green color highlights the drastic examples of chromatin clustering impaired mutants. (**B**) Structure of the MBD (in yellow) of MeCP2 in complex with DNA (in white) is displayed as in Figure 1A, and the residues are color coded as in (A). β-Strands (β1 and β2), α-helix (α1), loops (L1, L2, L3) and the Asx-ST motif are marked. The NH_2-terminal part of the protein structure is indicated.

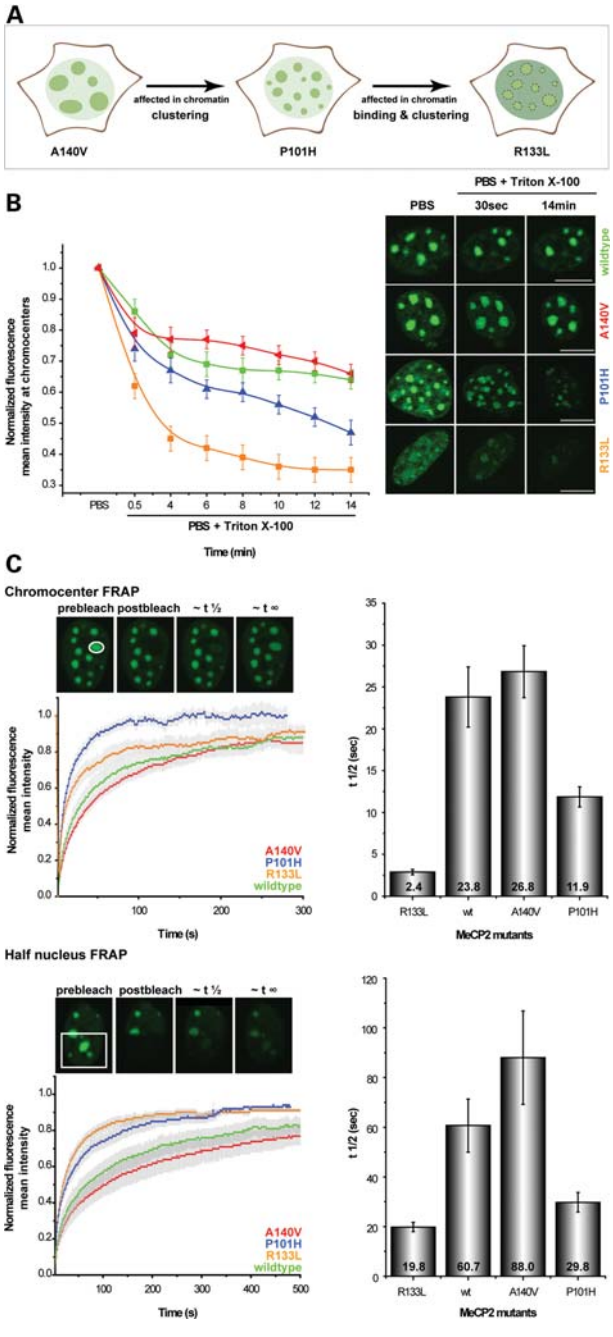

Figure 4. MeCP2 Rett mutant proteins show different kinetics *in vivo*. (**A**) Schematic representation of cells expressing selected Rett mutants defective in binding or clustering of heterochromatin. (**B**) *In situ* extraction kinetics for GFP-tagged proteins was performed by permeabilizing the cells on the microscope stage with Triton X-100 and measuring the decrease in protein at chromocenters over time. The experiment was repeated twice and 7–10 cells were analyzed each time, for each mutant. The line graph shows the extraction kinetics of the mutants over time. Error bars represent the standard error of the mean, and representative mid section images are shown on the right. Scale bar represents 10 μm. (**C**) FRAP curves of GFP-tagged wild-type and mutant MeCP2 together with representative images before and after photobleaching. For FRAP analysis, either a whole chromocenter or half of the nucleus (marked in white) was photobleached. The experiments were repeated two times with 10–20 cells photobleached per construct each time. Results were averaged and the mean curve as well as the standard error of the mean was calculated. Half times of recovery shown on the bar histograms were calculated from the mean curves and the error bars represent the standard error of the mean.

higher contribution of the nucleoplasmic MeCP2 fraction) or was measured in human cells (Supplementary Material, Fig. S2C).

Since the P101 is located far away from the 5 mC interacting pocket, these data suggest that it is primordially involved in connecting chromatin fibers most likely through interactions with other chromatin proteins. From all the MBD residues, the P101 seems particularly sensitive to any substitution (Fig. 1A). Whereas mutations to L, S and T have a mild heterochromatin clustering effect, substitution to positively charged residues (R or H) results in a drastic effect. This residue is located in the NH_2-terminal part of the MBD and likely induces a sharp turn before the two opposing β-sheets (β1 and β2, Fig. 1). Interference with this rigid proline-induced conformation may be more significant on replacement with the not very flexible histidine and less with the other more malleable amino acids. The same could apply for the P152 substitution to the basic residue R.

In summary, our analysis of the *in vivo* chromocenter clustering ability of the different mutations clearly indicated that all mutants where this property was significantly disrupted mapped to the same outer surface of the MBD structure and, significantly, these mutants were not concomitantly affected in chromatin binding *per se*. From the chromocenter accumulation analysis, we conclude that such mutants should be able to bind well to DNA/chromatin *in vivo*, but could be affected in interactions to other heterochromatin proteins and, thus, could not induce chromocenter clustering resulting in faster FRAP kinetics. When compared with other chromatin binders, the FRAP kinetics of wild-type MeCP2 are much faster than the core histone components (22) but close to the kinetics of the linker histone H1 (23,24). Indeed, both MeCP2 and histone H1 compete for binding to nucleosomes *in vitro* (25,26) and bind to the linker DNA (14,27,28). Moreover, MeCP2 is able to condense chromatin *in vitro* to the same level as histone H1 and under physiological salt concentrations (7). These *in vitro* data suggest that MeCP2 can 'cross-link' chromatin fibers together as is the case with the linker histone H1. On the other hand, other stereotypical heterochromatin proteins, such as HP1α, are highly mobile and have a much faster exchange on chromatin (Supplementary Material, Fig. S3) (29–32). We have previously shown that MeCP2 but not HP1α clusters chromatin *in vivo* (5,6) and our present data suggest that mutations occurring in Rett patients are defective in the chromatin architecture function of MeCP2.

We therefore propose that proteins involved in the formation and stabilization of higher-order chromatin structures ('chromatin linkers') bind to chromatin through multiple modes of interactions including, in the case of MeCP2, interactions with 5 mC, DNA and other chromatin proteins and have a longer residence time on chromatin. The latter might also conversely facilitate the establishment of multiple higher-order contacts in a self-reinforcing loop. We suggest that the cooperation of all these binding modes, which individually may have low affinity, promotes ultimately stable association of MeCP2 at heterochromatin, measured in the FRAP and *in situ* extraction experiments. This stable binding could facilitate connections within and between chromatin fibers and lead to a dynamic yet stable organization of heterochromatin

domains with a modulating effect on the level of transcriptional noise. Less stable MeCP2 heterochromatin binding and/or smaller heterochromatin domains within the nucleus could conceivably play a role in Rett syndrome etiology.

MATERIALS AND METHODS

Expression plasmids

Expression vectors encoding GFP-tagged fusions of human wild-type or mutant MeCP2 cDNA cloned into the pEGFP-C1 vector were described before (17) as was GFP-HP1α (32).

Cell culture, transfection and staining

Pmi28 mouse myoblasts were cultured as described (33). Cells were plated on glass coverslips or multiwell dishes (ibidi μ-dishes 8 well; Ibidi GmbH, Munich, Germany) prior to transfection for fixed cell or live cell experiments, respectively. Cells were transfected using TransFectin™ (Bio-Rad, Hercules, CA, USA) following the manufacturer's protocol. Cultures were fixed and DNA stained as described (6). In short, cultures were rinsed in phosphate-buffered saline (PBS) and fixed in 3.7% formaldehyde in PBS. Nuclear DNA was counterstained using TOPRO-3 (Invitrogen, Carlsbad, CA, USA), Hoechst 33258 or DAPI, and samples were mounted in vectashield antifading medium (Vector Laboratories, Burlingame, CA, USA) or moviol.

Microscopy and image analysis

For chromocenter counting, cells were fixed and examined on a Zeiss Axiovert 200 epifluorescence microscope. Image stacks (0.5 μm Z-interval) were acquired with a 63× Plan-Apochromatic NA 1.4 or 40× Plan-Neofluar NA 1.3 oil immersion phase contrast objectives and a PCO Sensicam QE cooled CCD camera. The image stacks were analyzed using a semi-automated approach. For this, we developed a custom application using the priithon platform. Image stacks were treated as three-dimensional volumes and segmented displaying an optical section view and a maximum intensity Z-projection. Nuclei and chromocenters were automatically identified by intensity-based thresholding and implementation of the water algorithm (34). Identified nuclei and chromocenters were outlined and numbered and the performance of the algorithm was controlled by visual inspection using optical section views and maximum intensity Z-projections. Parameters were adjusted to account for different sample brightness and chromocenter density. All intermediate images, parameters and counting results were automatically saved. Cumulative frequencies of chromocenter numbers were tested for statistical significance utilizing the Kolmogorov–Smirnov test.

To assess the chromocenter binding ability, we collected confocal Z stacks (voxel size: 0.05 × 0.05 × 0.3 μm) of formaldehyde-fixed cells expressing similar levels of the GFP fusion protein on either Zeiss LSM510Meta or Leica SP5 confocal microscopes, using 63×/1.4 NA oil objective and 405 nm diode pumped solid state (for Hoechst 33258, DAPI), 488 nm Argon (for GFP) and 633 nm He-Ne (TOPRO-3) laser excitation. Care was taken in selecting the imaging conditions to avoid under- and overexposed pixels, while keeping the imaging conditions constant. Heterochromatic foci were identified by counterstaining with TOPRO-3, Hoechst 33258 or DAPI. Image analysis was performed using ImageJ version 1.38× (http://rsb.info.nih.gov/ij; last accessed: 15.08.2011). The average mean intensity at the chromocenters versus the nucleoplasm was assessed by selecting four regions of equal size in the two compartments, calculating the mean fluorescent intensity in each compartment and then taking the ratio between both. The formula used to calculate the accumulation of MeCP2 and mutants at chromocenters for each construct was:

$$\text{Accumulation at chromocenter} = \frac{\text{average mean intensity at chromocenters}}{\text{average mean intensity in nucleoplasm}}$$

In the case of chromocenter binding assays, statistical significance was checked through the *t*-test.

In situ extraction of GFP-tagged wild-type MeCP2 and MeCP2-bearing mutants was done by transfecting the cells plated on ibidi dishes with the respective construct and extracting them directly on the microscope while imaging. Cells were first washed with PBS containing 0.5 mM $MgCl_2$, 0.5 mM $CaCl_2$ and imaged. Then, the solution was changed to PBS containing 0.5 mM $MgCl_2$, 0.5 mM $CaCl_2$ and 0.5% Triton X-100. Confocal Z-series were recorded over time on a Zeiss LSM510Meta confocal microscope, using 63×/1.4 NA oil objective. The microscope was equipped with a microscope cage incubation chamber (Oko-lab, Ottaviano, Italy) and the temperature was maintained at 37°C. GFP was excited with the 488 nm argon laser line. Confocal Z-stacks were acquired with a frame size of 1024 × 1024 pixels (voxel size: 0.20 × 0.20 and 1.0 μm), at 2 min time intervals for 14 min. Quantitative evaluation was performed using ImageJ. The mean fluorescence intensities at the chromocenters for each cell and time point were calculated for PBS and PBS−Triton X-100. First, using ImageJ 'adjust threshold' plug-in, the chromocenters were identified and then 'create selection' plug-in was used to assess the mean fluorescence intensity only at chromocenters. This procedure was repeated for each cell and time point. The whole data set for each cell was then normalized to the mean fluorescence intensities of the chromocenters before extraction with Triton X-100. The results were evaluated using Microsoft Excel and plotted using Microsoft Excel or Origin 7.5 software (Origin Lab Corp.).

Fluorescence recovery after photobleaching

Live cell imaging and FRAP experiments were performed on an on a LSM510Meta confocal microscope (Zeiss) using a 63×/1.4NA Plan-Apochromat oil immersion objective. The microscope was maintained at 37°C with the help of an Oko-lab cage incubation chamber. Confocal image series were recorded with a frame size of 512 × 512 pixels (pixel size: 60 nm) and at 2 s time intervals; 488 nm argon laser

line (25 mW) was used at 100% transmission to bleach and at 0.05% transmission to record GFP-tagged proteins over time, with the pinhole opened to 3 Airy units. Either a whole chromocenter or half of the nucleus was photobleached, and 5–10 pre-bleach and 250–400 post-bleach frames were recorded for each time-series. Quantitative evaluation was performed using ImageJ and Microsoft Excel. Briefly, the time-series was first corrected for translational movements using 'stackreg' plug-in from ImageJ and the analysis of the FRAP data was performed exactly as described (35).

SUPPLEMENTARY MATERIAL

Supplementary Material is available at *HMG* online.

ACKNOWLEDGEMENTS

We are indebted to Ingrid Grunewald and Anne Lehmkuhl for excellent technical support. We are further grateful to Akos Dobay, Andrea Rottach, Garwin Pichler and Tino Dittrich for helpful discussion and advice and to Tom Misteli for the GFP-HP1α expression construct.

Conflict of Interest statement. None declared.

FUNDING

T.H. was supported by the European Union (ESF program). This work was funded by grants of the Deutsche Forschungsgemeinschaft and by the E-Rare EuroRETT network (BMBF) to M.C.C.

REFERENCES

1. Amir, R.E., Van den Veyver, I.B., Wan, M., Tran, C.Q., Francke, U. and Zoghbi, H.Y. (1999) Rett syndrome is caused by mutations in X-linked MECP2, encoding methyl-CpG-binding protein 2. *Nat. Genet.*, **23**, 185–188.
2. Nan, X., Tate, P., Li, E. and Bird, A. (1996) DNA methylation specifies chromosomal localization of MeCP2. *Mol. Cell. Biol.*, **16**, 414–421.
3. Jones, P.L., Veenstra, G.J., Wade, P.A., Vermaak, D., Kass, S.U., Landsberger, N., Strouboulis, J. and Wolffe, A.P. (1998) Methylated DNA and MeCP2 recruit histone deacetylase to repress transcription. *Nat. Genet.*, **19**, 187–191.
4. Nan, X., Cross, S. and Bird, A. (1998) Gene silencing by methyl-CpG-binding proteins. *Novartis Found. Symp.*, **214**, 6–16.; discussion 16–21, 46–50.
5. Brero, A., Easwaran, H.P., Nowak, D., Grunewald, I., Cremer, T., Leonhardt, H. and Cardoso, M.C. (2005) Methyl CpG-binding proteins induce large-scale chromatin reorganization during terminal differentiation. *J. Cell Biol.*, **169**, 733–743.
6. Agarwal, N., Hardt, T., Brero, A., Nowak, D., Rothbauer, U., Becker, A., Leonhardt, H. and Cardoso, M.C. (2007) MeCP2 interacts with HP1 and modulates its heterochromatin association during myogenic differentiation. *Nucleic Acids Res.*, **35**, 5402–5408.
7. Georgel, P.T., Horowitz-Scherer, R.A., Adkins, N., Woodcock, C.L., Wade, P.A. and Hansen, J.C. (2003) Chromatin compaction by human MeCP2. Assembly of novel secondary chromatin structures in the absence of DNA methylation. *J. Biol. Chem.*, **278**, 32181–32188.
8. Archer, H.L., Whatley, S.D., Evans, J.C., Ravine, D., Huppke, P., Kerr, A., Bunyan, D., Kerr, B., Sweeney, E., Davies, S.J. *et al.* (2006) Gross rearrangements of the MECP2 gene are found in both classical and atypical Rett syndrome patients. *J. Med. Genet.*, **43**, 451–456.
9. Pan, H., Li, M.R., Nelson, P., Bao, X.H., Wu, X.R. and Yu, S. (2006) Large deletions of the MECP2 gene in Chinese patients with classical Rett syndrome. *Clin. Genet.*, **70**, 418–419.
10. Chahrour, M. and Zoghbi, H.Y. (2007) The story of Rett syndrome: from clinic to neurobiology. *Neuron*, **56**, 422–437.
11. Tudor, M., Akbarian, S., Chen, R.Z. and Jaenisch, R. (2002) Transcriptional profiling of a mouse model for Rett syndrome reveals subtle transcriptional changes in the brain. *Proc. Natl Acad. Sci. USA*, **99**, 15536–15541.
12. Nectoux, J., Fichou, Y., Rosas-Vargas, H., Cagnard, N., Bahi-Buisson, N., Nusbaum, P., Letourneur, F., Chelly, J. and Bienvenu, T. (2010) Cell cloning-based transcriptome analysis in Rett patients: relevance to the pathogenesis of Rett syndrome of new human MeCP2 target genes. *J. Cell. Mol. Med.*, **14**, 1962–1974.
13. Urdinguio, R.G., Lopez-Serra, L., Lopez-Nieva, P., Alaminos, M., Diaz-Uriarte, R., Fernandez, A.F. and Esteller, M. (2008) Mecp2-null mice provide new neuronal targets for Rett syndrome. *PLoS One*, **3**, e3669.
14. Nikitina, T., Ghosh, R.P., Horowitz-Scherer, R.A., Hansen, J.C., Grigoryev, S.A. and Woodcock, C.L. (2007) MeCP2-chromatin interactions include the formation of chromatosome-like structures and are altered in mutations causing Rett syndrome. *J. Biol. Chem.*, **282**, 28237–28245.
15. Kumar, A., Kamboj, S., Malone, B.M., Kudo, S., Twiss, J.L., Czymmek, K.J., LaSalle, J.M. and Schanen, N.C. (2008) Analysis of protein domains and Rett syndrome mutations indicate that multiple regions influence chromatin-binding dynamics of the chromatin-associated protein MECP2 *in vivo*. *J. Cell Sci.*, **121**, 1128–1137.
16. Marchi, M., Guarda, A., Bergo, A., Landsberger, N., Kilstrup-Nielsen, C., Ratto, G.M. and Costa, M. (2007) Spatio-temporal dynamics and localization of MeCP2 and pathological mutants in living cells. *Epigenetics*, **2**, 187–197.
17. Kudo, S., Nomura, Y., Segawa, M., Fujita, N., Nakao, M., Schanen, C. and Tamura, M. (2003) Heterogeneity in residual function of MeCP2 carrying missense mutations in the methyl CpG binding domain. *J. Med. Genet.*, **40**, 487–493.
18. Orrico, A., Lam, C., Galli, L., Dotti, M.T., Hayek, G., Tong, S.F., Poon, P.M., Zappella, M., Federico, A. and Sorrentino, V. (2000) MECP2 mutation in male patients with non-specific X-linked mental retardation. *FEBS Lett.*, **481**, 285–288.
19. Ohki, I., Shimotake, N., Fujita, N., Nakao, M. and Shirakawa, M. (1999) Solution structure of the methyl-CpG-binding domain of the methylation-dependent transcriptional repressor MBD1. *EMBO J.*, **18**, 6653–6661.
20. Ho, K.L., McNae, I.W., Schmiedeberg, L., Klose, R.J., Bird, A.P. and Walkinshaw, M.D. (2008) MeCP2 binding to DNA depends upon hydration at methyl-CpG. *Mol. Cell*, **29**, 525–531.
21. Tsumura, A., Hayakawa, T., Kumaki, Y., Takebayashi, S., Sakaue, M., Matsuoka, C., Shimotohno, K., Ishikawa, F., Li, E., Ueda, H.R. *et al.* (2006) Maintenance of self-renewal ability of mouse embryonic stem cells in the absence of DNA methyltransferases Dnmt1, Dnmt3a and Dnmt3b. *Genes Cells*, **11**, 805–814.
22. Kimura, H. (2005) Histone dynamics in living cells revealed by photobleaching. *DNA Repair (Amst.)*, **4**, 939–950.
23. Misteli, T., Gunjan, A., Hock, R., Bustin, M. and Brown, D.T. (2000) Dynamic binding of histone H1 to chromatin in living cells. *Nature*, **408**, 877–881.
24. Lever, M.A., Th'ng, J.P., Sun, X. and Hendzel, M.J. (2000) Rapid exchange of histone H1.1 on chromatin in living human cells. *Nature*, **408**, 873–876.
25. Ghosh, R.P., Horowitz-Scherer, R.A., Nikitina, T., Shlyakhtenko, L.S. and Woodcock, C.L. (2010) MeCP2 binds cooperatively to its substrate and competes with histone H1 for chromatin binding sites. *Mol. Cell. Biol.*, **30**, 4656–4670.
26. Nan, X., Campoy, F.J. and Bird, A. (1997) MeCP2 is a transcriptional repressor with abundant binding sites in genomic chromatin. *Cell*, **88**, 471–481.
27. Ishibashi, T., Thambirajah, A.A. and Ausio, J. (2008) MeCP2 preferentially binds to methylated linker DNA in the absence of the terminal tail of histone H3 and independently of histone acetylation. *FEBS Lett.*, **582**, 1157–1162.

28. Chandler, S.P., Guschin, D., Landsberger, N. and Wolffe, A.P. (1999) The methyl-CpG binding transcriptional repressor MeCP2 stably associates with nucleosomal DNA. *Biochemistry*, **38**, 7008–7018.
29. Schmiedeberg, L., Weisshart, K., Diekmann, S., Meyer Zu Hoerste, G. and Hemmerich, P. (2004) High and low mobility populations of HP1 in heterochromatin of mammalian cells. *Mol. Biol. Cell.*, **15**, 2819–2833.
30. Phair, R.D., Scaffidi, P., Elbi, C., Vecerova, J., Dey, A., Ozato, K., Brown, D.T., Hager, G., Bustin, M. and Misteli, T. (2004) Global nature of dynamic protein–chromatin interactions *in vivo*: three-dimensional genome scanning and dynamic interaction networks of chromatin proteins. *Mol. Cell. Biol.*, **24**, 6393–6402.
31. Festenstein, R., Pagakis, S.N., Hiragami, K., Lyon, D., Verreault, A., Sekkali, B. and Kioussis, D. (2003) Modulation of heterochromatin protein 1 dynamics in primary mammalian cells. *Science*, **299**, 719–721.
32. Cheutin, T., McNairn, A.J., Jenuwein, T., Gilbert, D.M., Singh, P.B. and Misteli, T. (2003) Maintenance of stable heterochromatin domains by dynamic HP1 binding. *Science*, **299**, 721–725.
33. Kaufmann, U., Kirsch, J., Irintchev, A., Wernig, A. and Starzinski-Powitz, A. (1999) The M-cadherin catenin complex interacts with microtubules in skeletal muscle cells: implications for the fusion of myoblasts. *J. Cell Sci.*, **112 (Pt 1)**, 55–68.
34. Harmon, B. and Sedat, J. (2005) Cell-by-cell dissection of gene expression and chromosomal interactions reveals consequences of nuclear reorganization. *PLoS Biol.*, **3**, e67.
35. Schermelleh, L., Haemmer, A., Spada, F., Rosing, N., Meilinger, D., Rothbauer, U., Cardoso, M.C. and Leonhardt, H. (2007) Dynamics of Dnmt1 interaction with the replication machinery and its role in postreplicative maintenance of DNA methylation. *Nucleic Acids Res.*, **35**, 4301–4312.

MeCP2 Rett mutations affect large scale chromatin organization

Noopur Agarwal[1#], Annette Becker[2#], K. Laurence Jost[1,2], Sebastian Haase[1], Basant K. Thakur[3], Alessandro Brero[1], Tanja Hardt[1], Shinichi Kudo[4], Heinrich Leonhardt[5] and M. Cristina Cardoso[1,2,*]

[1]Max Delbrück Center for Molecular Medicine, 13125 Berlin, Germany

[2]Department of Biology, Technische Universität Darmstadt, 64287 Darmstadt, Germany

[3]Department of Pediatric, Hematology and Oncology, Medical School Hannover, 30625 Hannover, Germany

[4]Hokkaido Institute of Public Health, Sapporo, 060-0819, Japan

[5]Department of Biology, Ludwig Maximilians University Munich, 82152 Planegg-Martinsried, Germany

# these authors contributed equally to this work

* M. Cristina Cardoso, Department of Biology, Technische Universität Darmstadt, Schnittspahnstr. 10, D-64283 Darmstadt, Germany, Telephone +49-6151-162377, Fax +49-6151-162375, E-mail cardoso@bio.tu-darmstadt.de

Present address:

Noopur Agarwal: BRIC-Biotech Research & Innovation Center, 2200 Copenhagen, Denmark

Sebastian Haase: Department of Physics, Freie Universität Berlin, 14195 Berlin, Germany

Tanja Hardt: Medical Proteomics Center, Ruhr University, 44801 Bochum, Germany

Supplemental figures:

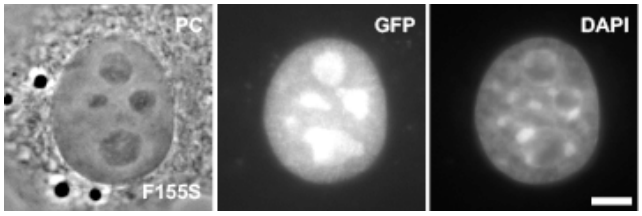

Figure S1: F155S mutant mislocalizes to the nucleolus and is deficient in heterochromatin binding and clustering. Cells were transfected, formaldehyde fixed and DNA was counterstained with DAPI. Representative epifluorescence images of a mouse cell expressing the GFP-tagged MeCP2 mutant are shown. PC: phase contrast. Scale bar: 5 µm.

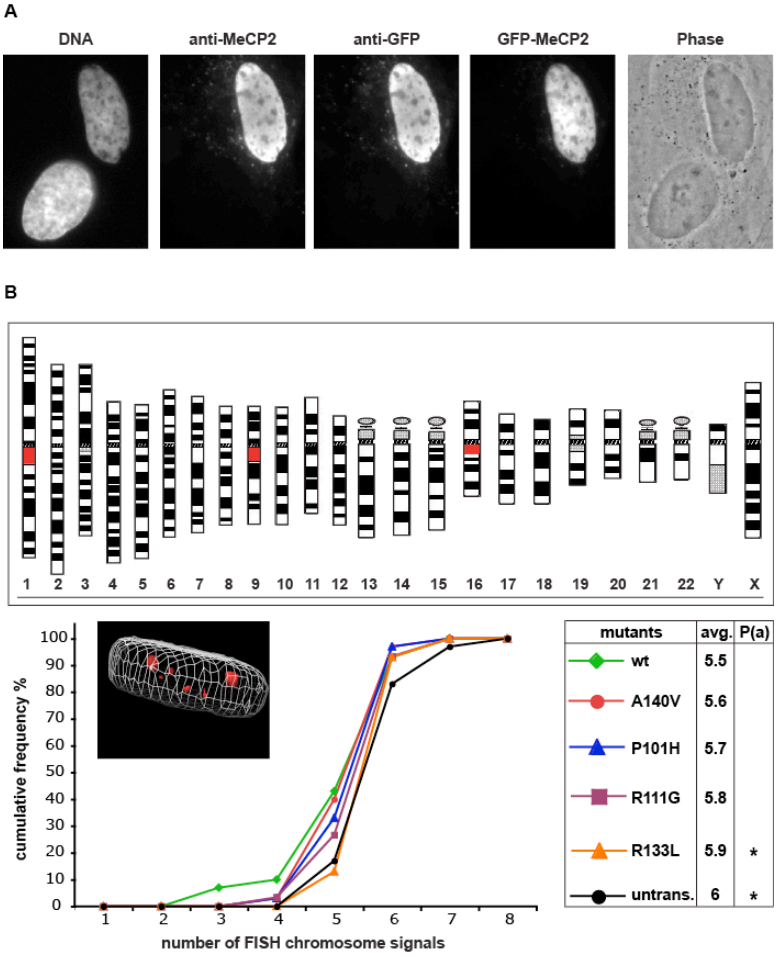

Figure S2: MeCP2 induces heterochromatin clustering in human diploid cells. Human foreskin diploid fibroblasts (Bj-hTERT) were transfected with a plasmid encoding for GFP-tagged human MeCP2, fixed after 12h and immunostained with anti-MeCP2 and anti-GFP. The image shows one exemplary field including one transfected cell identified by direct GFP fluorescence as well as anti-GFP and anti-MeCP2 antibody staining. The second cell was not transfected and hence shows no GFP or anti-GFP signals. The lack of any signal with the MeCP2-specific antibody in the untransfected cells indicates that Bj-hTERT cells, similar to Pmi28 cells, do not contain detectable levels of endogenous MeCP2. (B) Top panel: ideogram of G-banded human chromosomes (www.pathology.washington.edu/galleries/cytogallery/main.php?file=human%20karyotypes). Chromosomes 1, 9 and 16 were selected for our analysis as they contain the largest pericentric heterochromatin regions (marked in red). Bottom panel: Cells were transfected with constructs coding for GFP-tagged wild type and mutant human MeCP2 and clustering of these heterochromatic regions was analyzed by simultaneous hybridization with three DNA probes from the pericentric heterochromatin DNA of the three indicated chromosomes. Cells expressing the GFP-tagged MeCP2 protein were identified by immunostaining with anti-MeCP2 antibody and DNA was counterstained with DAPI. Confocal Z stacks of images from the GFP-MeCP2 signal, overall DNA signal and DNA FISH probes were then acquired. The three dimensional rendering of one such cell is shown where the contour of the nucleus is depicted by the white grid and the FISH signals of the three pericentric heterochromatin regions in red. The cumulative frequency of the

FISH signals counted is shown by the graph. The table lists the average number of chromosome signals and presents the p value (t-test) through asterisks representing statistically significant difference in regard to the wild type: * for P<0.05. Experiments were repeated twice with 30 cells evaluated each time per construct. (C) FRAP and the corresponding kinetic data analysis on the MeCP2 and mutants expressed in human Bj-hTERT cells. Half times of recovery were calculated from the mean curves and are shown in the bar chart. The error bars represent the standard error of the mean. The experiment was repeated twice with 15-20 cells evaluated each time per construct.

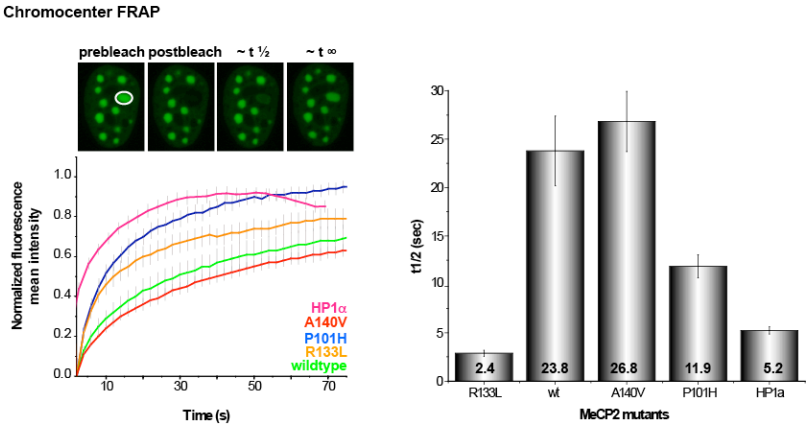

Figure S3: Comparison of heterochromatin binding kinetics of MeCP2 Rett mutants and HP1. FRAP curves of GFP-tagged wild type, mutant MeCP2 and HP1α expressed in Pmi28 cells. Experiments were repeated two times with 10-20 cells photobleached each time. Results were averaged and the mean curve and standard error of the mean were calculated. Half times were determined from the mean curves and are shown in the bar chart together with standard error of the mean.

Supplemental methods:

Human cell culture and transfection

The human foreskin fibroblast (Bj-hTERT) cell line (ATCC BJ-5ta) was derived by transfection of human foreskin fibroblasts with the pGRN145 hTERT expression plasmid and selection of stable immortalized cell clones (1). It is a diploid human cell line with a modal chromosome number of 46 that occurred in 90% of the cells counted and karyotypically normal X and Y sex chromosomes.

Human Bj-hTERT fibroblasts were cultured in DMEM medium containing 10% FCS, glutamine and gentamicin. Cells were transfected using the Amaxa nucleofactor (Amaxa AG, Cologne, Germany) or TransFectin™ (BioRad, Hercules, CA) following the manufacturer's protocols.

ImmunoFISH

For fluorescence *in situ* hybridization, the following DNA probes were used: repetitive specific human DNA probe pUC 1.77 (2) for chromosome 1, alphoid DNA probe pMR9A for the centromeric region 9q12 of chromosome 9 and alphoid DNA probe pHUR-195 for the centromeric region 16q11.2 of chromosome 16. These DNA probes were labeled by standard nick translation with Cy5-dUTP (Amersham, Buckinghamshire, UK). The labeled DNA was further purified by ethanol-precipitation and the pellet resuspended in hybridization solution (70% formamide, 2xSSC, 10% dextran sulfate, pH 7.0). The probes were denatured at 80 °C for 5 minutes.

For immunoFISH cells were fixed with 4% paraformaldehyde in PBS for 10 minutes and

permeabilized with 0.25% Triton X-100 in PBS for another 10 minutes. Primary (rabbit polyclonal anti-MeCP2) and secondary (anti-rabbit IgG Alexa Fluor 568; Molecular probes, CA, USA) antibodies were diluted in PBS with 0.2% fish skin gelatin and incubated sequentially for one hour each at room temperature. After immunostaining, the cells are post-fixed with 4% paraformaldehyde for 60 minutes followed by post-permeabilization with 0.5% Triton X-100 in PBS for 10 minutes, 0.1 M HCl for 10 minutes and 20% glycerol for 4 minutes. Probes were added to the cells and sealed with rubber cement to decrease evaporation of the probe over night. They were then denatured simultaneously at 75 °C for 5 minutes and hybridized over night at 37 °C. Non-hybridized probe was washed off using 50% formamide in SSC at 45 °C three times followed by two washes with 2xSSC. DNA was counterstained with DAPI and the cells were mounted using vectashield.

MeCP2 expressing cells were identified by the positive staining with anti-MeCP2 antibody and complete Z stacks of images (voxel size: 80 x 80 x 200 nm) of the DAPI (excited at 405 nm) and Cy5 (excited at 633 nm) signals for whole DNA and chromosomes 1, 9 and 16 pericentric heterochromatin regions, respectively, were acquired on a Leica SP5 laser scanning microscope using a 63x/1.4NA oil objective.

FISH signals were counted manually through these stacks. 3D rendering was done using UCSF chimera (www.cgl.ucsf.edu/chimera).

Supplemental references:

1 Bodnar, A.G., Ouellette, M., Frolkis, M., Holt, S.E., Chiu, C.P., Morin, G.B., Harley, C.B., Shay, J.W., Lichtsteiner, S. and Wright, W.E. (1998) Extension of life-span by introduction of telomerase into normal human cells. *Science*, **279**, 349-352.

2 Cooke, H.J. and Hindley, J. (1979) Cloning of human satellite III DNA: different components are on different chromosomes. *Nucleic Acids Res*, **6**, 3177-3197.